Hindawi
Advances in Materials Science and Engineering
Volume 2022, Article ID 9174538, 12 pages
https://doi.org/10.1155/2022/9174538

Research Article

Green Synthesis Ca-MgO Nanosorbent for the Uptake of Cobalt Ions from Aqueous Media

Noha Al-Awaji,[1] Moufida Boukriba,[2] Hajo Idriss,[3] Mohamed Ali Ben Aissa,[2] Mohamed Bououdina,[4] and Abueliz Modwi[2]

[1]*Department of Chemistry, College of Science, Qassim University, Buraidah 51452, Saudi Arabia*
[2]*Department of Chemistry, College of Science and Arts, Qassim University, Al-Rass 51921, Saudi Arabia*
[3]*Physics Department, College of Science, Imam Mohammad Ibn Saud Islamic University (IMSIU), Riyadh 13318, Saudi Arabia*
[4]*Department of Mathematics and Sciences, Faculty of Humanities and Sciences, Prince Sultan University, Riyadh 12435, Saudi Arabia*

Correspondence should be addressed to Mohamed Bououdina; mbououdina@psu.edu.sa and Abueliz Modwi; abuelizkh81@gmail.com

Received 23 July 2022; Revised 21 November 2022; Accepted 6 December 2022; Published 31 December 2022

Academic Editor: Marco Cannas

Ca-doped magnesium oxide nanosorbent has been prepared by sol-gel in the presence of gum arabic extract and assessed for the removal of cobalt ions (Co (II)) from aqueous media. X-ray diffraction analysis indicates the formation of MgO and CaO composites with a mean crystallite size of 6 nm having a large surface area of 50 m^2/g. Scanning and transmission electron microscopy observations reveal spherical-shaped particles at the nanoscale around 20 nm. Besides, X-ray photoelectron spectroscopy and Fourier transform infrared analyses manifest the existence of functional groups, which will facilitate the adsorption of metal ions. The adsorption capability of the CaO-MgO nanosorbent achieved 469.5 mg/g for Co (II) ions under optimum operating conditions. Furthermore, the experimental data elucidate that the adsorption process is primarily diffusion-based and that both intraparticle and boundary layer diffusion appear to play a key role in the rate-controlling step. The findings of this study highlight the remediation of contaminated water by cobalt ions by CaO-MgO nanostructure and can be extended to other metal ions and organic pollutants.

1. Introduction

Cobalt is a naturally occurring chemical element with an atomic number of 27, belongs to the *d* sublevel elements, and is located at the top of the ninth group of elements in the periodic table, chemically classified as a transition metal [1, 2]. Cobalt is found in nature, mainly in the Earth's crust in various minerals such as cobaltite, and it is not found in its natural, free form [3]. In contrast, the free element is produced from the reductive smelting of its ores. On the other hand, the pure state is found in the form of shiny silver-gray metal [4, 5]. Additionally, cobalt has been found to be a component of vitamin B_{12}, which plays a significant role in blood pressure regulation and thyroid function [6].

Nowadays, water contamination by heavy metals is one of the most critical and challenging environmental problems facing the world [7]. In particular, cobalt (II) is a nonbiodegradable, cancerous, and pathogenic contaminant found in natural, industrial, and artificial processes [8]. Cobalt is a metal used in various industries, including nuclear medicine, surface coatings, optoelectronics, milling machines, glassware and ceramic decorating, and metal processing [9]. Furthermore, it is also used as a drier for lacquers, varnishes, paints, and foaming stabilization in beer [10]. The continual release of various cobalt effluents from multiple industries endangers the environment and harms human health [11]. Cobalt (II) contamination of wastewater is a serious issue due to its toxicity at higher levels [12]. Cobalt has many

adverse health consequences, including cardiovascular disease, asthma, heart failure, goiter, and liver disorders [13].

Humans require water to survive; however, the quality of water available is insufficient to meet their basic needs [14]. Therefore, the quality control of water that has been contaminated with metal ions including Co (II) has become an increasingly important concern in recent years [15]. Numerous physicochemical approaches have been developed to effectively remove Co (II) ions from wastewater [16, 17], such as adsorption, membrane filtration, sedimentation, coprecipitation, and biotechnology [18, 19]. However, most of these technologies have substantial drawbacks such as low removal efficiency, high costs, operating requirements sensitivity, and secondary effluent generation [20]. Nonetheless, the adsorption method is considered the most suitable for removing Co (II) ions because of its low cost and high efficiency even in small quantities [21]. On the other hand, traditional sorbents have a limited binding capability and insufficient active surface sites, resulting in poor regeneration of particular metal ions from massive volumes of solution [22]. Consequently, the search for novel adsorbents with enhanced characteristics including high surface area, high efficiency, and fast segregation for vast volumes is of great importance [23].

Metallic oxide nanoparticles have been extensively investigated as potential sorbents, thanks to their exceptional characteristics and high efficacy [24, 25]. In this regard, magnesium oxide (MgO) has been examined due to its high capacity for the removal of metal ions in aqueous solutions [26, 27]. Recently, nanosized MgO nanoparticles have been wieldy used as nanosorbent to remediate contaminated water, owing to the large surface area and negligible impact on the environment [28, 29]. Furthermore, the adsorption capacity of MgO nanoparticles can be improved by surface modifications through physical coatings, alloying, doping, and covalent bonding to enable specific metal complexes [30, 31].

Green synthesis has been adopted by using the extract of the Acacia Senegal plant as a reducing and capping agent. The aim of this research is to synthesize Ca-doped MgO (CaO.MgO) nanopowder by the sol-gel method in the presence of Acacia Senegal solution and to examine its performance for the removal of Co (II) ions from aqueous solution. XRD, BET, FTIR, and SEM characterizations are performed for the removal of Co (II) ions from an aqueous solution. XRD, BET, FTIR, and SEM characterizations are performed in order to determine the phase composition, chemical bondings, surface properties, and particle morphology and size. The influence of the operating parameters such as Co (II) concentration, contact time, and pH on the adsorption capacity of Ca-doped MgO nanosorbent is also investigated. Furthermore, kinetic and isotherm adsorption tests are performed, the obtained data are modelled, and subsequently, a plausible adsorption mechanism is proposed.

2. Experimental Process

Ca-doped MgO oxide nanopowder was synthesized using by green sol-gel method aided by the Acacia Senegal solution. A 0.5 L of distilled water (DW) was dissolved in 0.249 mol. of magnesium carbonate dehydrate ($MgCO_3$) and 0.0249 mol. of calcium carbonate ($CaCO_3$). Then, 125 mL of NaOH ethanolic solution (0.02 M) was added dropwise for 30 min during sonication. Subsequently, 25 mL gum arabic (Acacia Senegal) solution (5 g in 100 ml DW) was added followed by sonication for 15 min, and afterward, the mixture was allowed to stand for 24 h. The as-formed white gel was washed with DW and dried at 90°C for 5 h. The final product was then calcined at 700°C for 2 h.

A Rigaku Mini Flex 600 (Tokyo, Japan) diffractometer equipped with a CuK radiation source ($\lambda = 1.5418$) was used to identify the crystal structure and phase purity. The surface area and pore size of the nanopowder were determined using a Micrometric ASAP 2020 analyzer, and Brunauer, Emmett, and Teller (BET) formula as well as Lippens and de Boer's t-plot method. A Shimadzu FT-IR spectrometer was used to investigate the vibrational modes of the prepared nanopowder before and after Co (II) ions adsorption. Morphological observations were performed using scanning electron microscopy (SEM) by means of a JEOL JEM-6700F instrument equipped with electron dispersive X-ray spectroscopy (EDS) for the elemental chemical composition. Transmission electron microscopy (TEM) images were acquired at a 200 kV accelerating voltage using an FEI Tecnai G20 instrument. The surface chemical species were analyzed using the X-ray photoelectron spectroscopy (XPS) technique on a Thermo Scientific XPS (VG ESCALAB 220i-XL, UK) equipped with a monochromatic Al K (1486.6 eV) reference.

Adsorption experiments were conducted in a 25 mL glass vial containing 10 mg of nanosorbent powder and 25 mL of Co (II) ions at various concentrations (5, 15, 30, 45, 60, 100, and 200 ppm) under electromagnetic stirring for a contact time of 1440 min. Following the elimination equilibrium study, the mixture was centrifuged and separated to estimate the residual Co (II) ions concentration [29]:

$$Q_e = \frac{V}{w}\left(C_i - C_e\right), \tag{1}$$

where Q_e (mg/g) denotes the ability of Co (II) ions to be removed by the mass of sorbent nanopowder, and C_e denotes the equilibrium Co (II) concentration in mg/L.

The adsorption procedure was used to determine the rate of Co (II) removal by the as-prepared nanosorbent (Ca-doped MgO). A 150 mL of Co(II) volume was stirred with 60 mg of nanosorbent at an initial concentration of 60 ppm to investigate the kinetics and contact time. A small suspension volume was withdrawn at preset time intervals and then centrifuged to determine the residual Co (II) concentration. Then, the amount of Co (II) separated per gram of nanosorbent at every period (min) was calculated by applying the following equation [32]:

$$Q_t = \frac{V}{w}\left(C_i - C_t\right), \tag{2}$$

where Q_t (mg/g) is the capability of Co (II) to be removed per mass of nanosorbent (w (g)) at each time t (min), C_i and C_t are the Co (II) concentrations (ppm) before and after introducing Co (II) at each time, and V is the volume of the solution mixture (mL).

3. Results and Discussion

3.1. Ca-Doped MgO Nanosorbent Characteristics. Figure 1(a) depicts the XRD pattern of the as-prepared Ca-doped MgO-powdered sample. The major peaks located at $2\theta = 36.9$, 42.9, 62.2, 74.6, and 78.6° are indexed as (111), (200), (220), (311), and (222) reflections of MgO phase with a face-centered cubic-FCC rock-salt type structure (space group Fmm–No. 225 and lattice constant $a = 4.213$ Å) [33] and consistent with JCPDS card No. 78-0430. The two small peaks observed at $2\theta = 36.9$ and 42.9° are attributed to the gum arabic extract [34] whereas the remaining peaks at 2 = 32.3 and 53.9 are indexed as (110) and (202) reflections of the cubic CaO phase (space group Fmm–No. 225 and lattice parameter $a = 4.801$ Å) [35], in agreement with JCPDS card no. 77-2376. Hence, the as-prepared Ca-doped MgO is in fact a nanocomposite composed mainly of MgO and CaO phases. The crystallite size calculated using the Sherrer formula is found to be around 5.98 nm [36]; hence, a high surface area of the as-prepared nanopowder consequently enhanced adsorption efficiency.

For the fabrication of an effective adsorbent, such as CaO.MgO nanopowder, it is high desirable the presence of a large number of actives sites at particles' surface, besides a high surface area with large pore-volume. The nitrogen adsorption-desorption isotherm curves (Figure 1(b) (inset pore size)) demonstrate that the as-prepared CaO.MgO nanocomposite is a mesoporous material with an IUPAC class IV adsorption isotherm. The isotherm is connected to a type H1 hysteresis, implying a limited dispersion of homogeneous mesoporous particles and limited networking effects [37, 38]. The nanosorbent CaO.MgO possesses a relatively high surface area of 50 m^2/g with a total porous volume of 0.277 cc/g and an average pore size of 11.79 nm. The adsorbent's important surface area and porosity are expected to expose many adsorption sites, leading to a high adsorption capacity.

Furthermore, FTIR analysis was used to identify the chemical bonds and composition (purity) of the synthesized nanosorbent, see Figure 1(c). The broad band at 3465 cm^{-1} is assigned to the O–H group's asymmetric stretching [39], while the band at 1639 cm^{-1} corresponds to the adsorbed water molecule's –OH stretching mode [40]. The three bands observed at 1524, 1406, and 1056 cm^{-1} are associated with an unknown carbonate adsorbed on the nanoparticles' surface [41]. The unique band at 420 cm^{-1} is attributed to the Mg–O vibration mode [42], hence confirming the formation of the MgO phase. Meanwhile, the band at 871 cm^{-1} is related to CaO stretching [43]. The FTIR analysis corroborates with the XRD analysis by confirming the formation of CaO.MgO nanocomposite material.

The SEM image displayed in Figure 2(a) reveals irregular-shaped spherical crystalline particles at the nanoscale with dimensions approximately around 20 nm. The corresponding EDX spectrum (Figure 2(b)) manifests intense signals at 3.7, 1.2, and 0.5 keV corresponding to Ca, Mg, and O, respectively. No additional peaks can be detected signifying the purity of the as-prepared nanosorbent. Furthermore, according to the chemical composition shown as an inset in Figure 2(b), the weight proportions of the components are compatible with the initial chemical composition. The TEM images as illustrated in Figures 2(c) and 2(d) indicate the presence of irregular and spherical particles with dimensions around 20 nm, in good agreement with SEM analysis.

XPS analysis has been used to determine the chemical state of the elements on the surface of CaO.MgO nanostructure, see Figures 3(a)–3(d). Ca-2p, Mg-2p, O-1s, and O-2s peaks are detected in the recorded survey scan (Figure 3(a)). The existence of an Mg-2p peak at around 52.50 eV is attributed to surface magnesium in an oxidized state, indicating the formation of Mg-O [44]. The Ca-2p peaks at 348.13 and 351.2 eV correspond to the divalent oxidation states of calcium oxygen molecules (Ca-2p3/2 and Ca-2p1/2), confirming the existence of calcium oxide (CaO) [45, 46]. The three O-1s peaks observed at 531.4, 532.5, and 533.8 eV correspond to Ca-O, Mg-O, and hydroxyl group in water molecules, respectively (see Figure 3(b)) [47]. The peaks at 42.0 and 51.1 eV may be ascribed to the typical Mg-2p and Mg-2s peaks of the MgO phase as shown in Figure 3(c) [48]. Moreover, the O-1s peak at 533.8 eV confirms the Mg-O bonding (Figure 3(d)) [49, 50]. It can be concluded that XPS analysis indicates the presence of Ca, Mg, and O species only without any additional peaks belonging to impurities, which corroborates with the results obtained by XRD, FTIR, and EDS analyses. Furthermore, the XPS results indicate that CaO.MgO nanostructure' surface is hydroxylated, which is consistent with FTIR analysis (the strong band for the O-H group in FTIR indicates the hydroxylation of the nanostructure).

3.2. Co (II) Removal onto CaO.MgO Nanosorbent

3.2.1. Influence of the Initial Co (II) Concentration. The influence of the initial Co (II) concentration in the range of 5–200 mg/L on the adsorption efficiency of CaO.MgO nanosorbent has been examined under the following operating conditions: contact time 1440 min, room temperature, pH 5, 350 rpm stirring speed, and a sorbent dose 10 mg. As shown in Figure 4, increasing the starting Co (II) concentration from 5 to 200 mg/L improved the adsorption capacity significantly from 12.5 to 462.23 mg/g but reduced slightly the adsorption rate and elimination efficiency of Co (II) from 100 to 92.45%. These results indicate that at lower concentrations, Co (II) ions in the reaction medium interact more efficiently with the top layer of the sorbent particles due to the large amount of vacant active sites. On the contrary, the ratio of accessible sites for Co (II) ions declines with a further rise in the concentration attributed to potential binding saturation.

3.2.2. Influence of pH on Co (II) Removal by the Nanosorbent. The pH of the solution governs the sorption affinity of the adsorbent by tunning the type of charge on the surface of the adsorbent, speciation of the metal in the solution, and ionizing strength of the adsorbent [51]. The influence of pH can also be described through the point of zero charges (pHpzc). It is known that pHpzc refers to the pH at which the surface of the adsorbent has a zero net charge. The evolution of

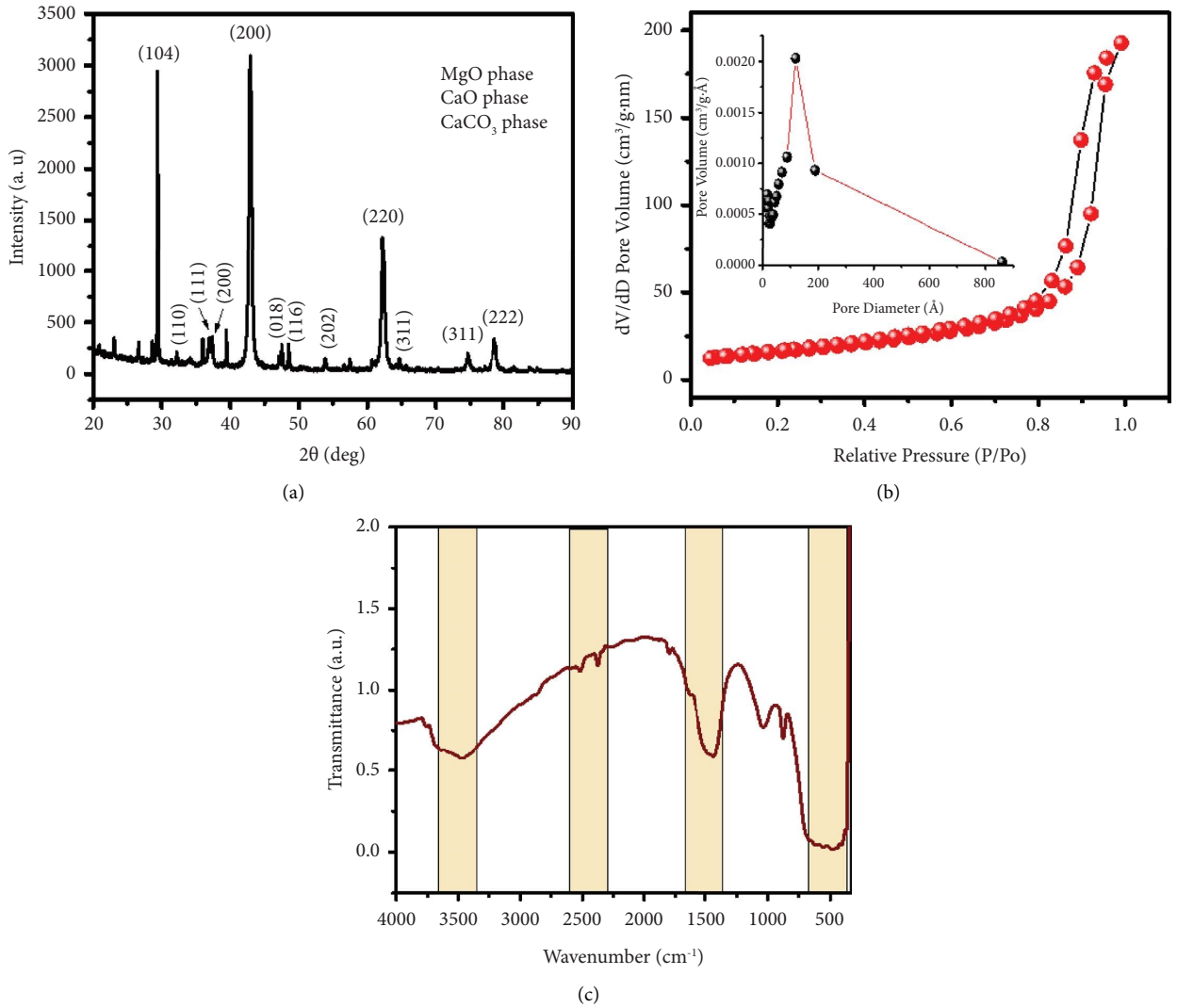

Figure 1: Characterization of Ca-MgO nanosorbent. (a) XRD pattern, (b) BET isotherm (inset pore distribution), and (c) FTIR of the fabricated CaO.MgO nanosorbent.

($pH_{final} - pH_{initial}$) *vs.* $pH_{initial}$, as illustrated in Figure 5(a), indicates that the value of pHpzc is 4.02. This result suggests that the surface of the adsorbent is positively charged and favors the sorption of anions for the solution with pHs < pHpzc (9.97). In contrast, it becomes negatively charged to favor the sorption of cations for the solution with pHs > pHpzc. To examine the optimal pH for the Co (II) removal, the pH has been varied from 1 to 8. The effect of pH on Co (II) uptake is depicted in Figure 5(b). As can be seen, the amount of the adsorbed Co (II) increases significantly reaching a maximum capacity of 130.36 mg/g at pH 5. Increasing pH reduces the amount of H^+, thus reducing competition for adsorption sites onto particle surfaces between metal ions and protons [52]. The other aspect that may aid in metal ions' sorption is the rise in the pH, which promotes their precipitation from solution as hydroxides. Consequently, the adsorption is reduced due to the formation of soluble hydroxyl complexes [53]. Hydroxonium ions (H_3O) may be tightly coupled with the surface of the adsorbent at low pH through a repulsive effect, leading to a decrease in metal ions elimination [54]. The Lewis base (lone pair electron) that is present in some of the functional groups of defatted CaO-MgO nanosorbent may play a significant role in eliminating metal ions by (Lewis acid) defatted CaO-MgO nanosorbent. The elimination of Co (II) from sewage by sorbents includes a more complex mechanism that is partly governed by sorption and chemical precipitation at the sewage-solid interface and the mechanism of its pore filling. Therefore, it is suggested that inner sphere complexes between CaO-MgO nanosorbent and metal ions may have formed. When hydroxyl groups occupy the place of metal ligands inside the inner coordination sphere, ions will undergo hydrolysis [55]. This replacement occurs following the removal of the metal cation-hydration outer sphere. Moreover, the findings of several studies in the literature corroborate the reported association between metal ions' adsorption and a more comprehensive pH range [56].

3.2.3. Effect of Co (II) Contact Time and Adsorption Kinetic Studies. Figure 6(a) depicts the correlation between Co (II) adsorption by CaO.MgO nanosorbent and the contact time.

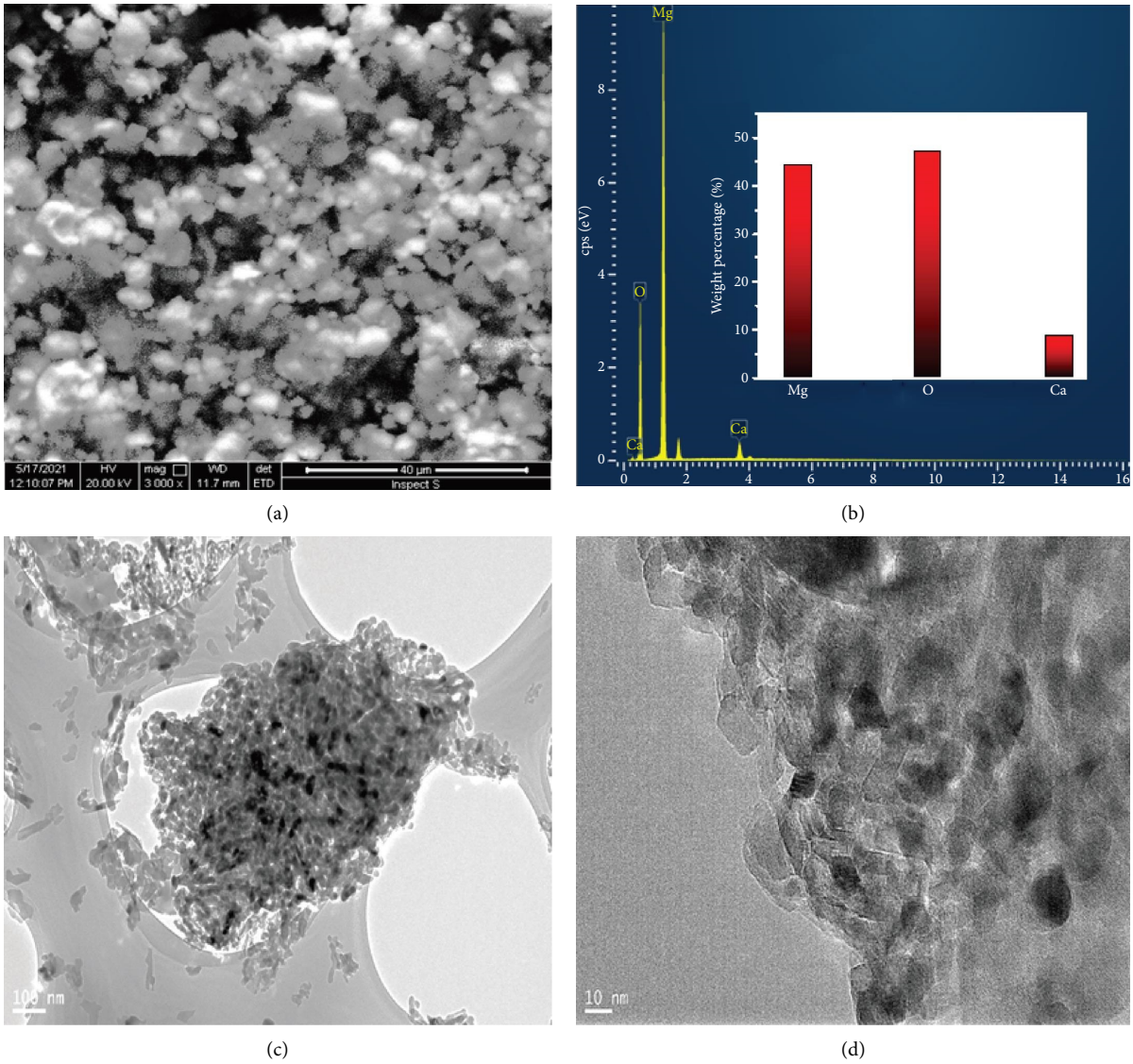

(a) (b)

(c) (d)

Figure 2: SEM image (a), EDX (b), and TEM images (c) and (d) of the prepared CaO.MgO nanosorbent.

The adsorption capacity and removal efficiency are found to increase with the contact time, reaching equilibrium at 18 min. Beyond this equilibrium threshold, the adsorption capacity is in dynamic equilibrium with the amount of adsorbed Co (II), as demonstrated by a negligible rise in Co (II) percentage. The first % elimination of Co (II) is rapid (Figure 6(a)), owing to a large number of adsorbent's active sites and the short diameter of Co (II) ions. After 18 min, Co (II) ions cannot penetrate the adsorbent's inner pores, which are attributed to Co (II) monomolecular saturation at the pores' surface. Additionally, the data from Figure 6(a) manifest that the equilibrium period is unrelated to the original Co (II) concentration.

The adsorption kinetics quantifies the rate of solute adsorption at the solid-liquid interface and provides critical information on the equilibrium time, which is necessary for the design and operation of an adsorption process [57]. Co (II) adsorption kinetics by the CaO.MgO nanosorbent has been examined by adopting pseudo-first-order (PFO) and pseudo-second-order (PSO) kinetic models as displayed in Figures 6(b) and 6(c). On the basis of the adsorbent capacity, a pseudo-first-order model is established. It states that the rate at which adsorbate consumption changes with time is directly proportional to the difference in saturation concentration levels. The corresponding equation's linear form is denoted in Table 1.

Table 1 summarizes the calculated model parameters under the studied experimental conditions. Although the fitted model has a high R^2 value of 0.9038, the computed Q_{max} value for initial Co (II) concentrations differs significantly from the experimental Q_{max} values. This discrepancy implies that the pseudo-first-order equation may not sufficiently describe the Co (II) adsorption pathway onto the surface of CaO.MgO nanoparticles, implying the necessity to examine the effectiveness by testing another kinetic model. The pseudo-second-order model may appropriately explain

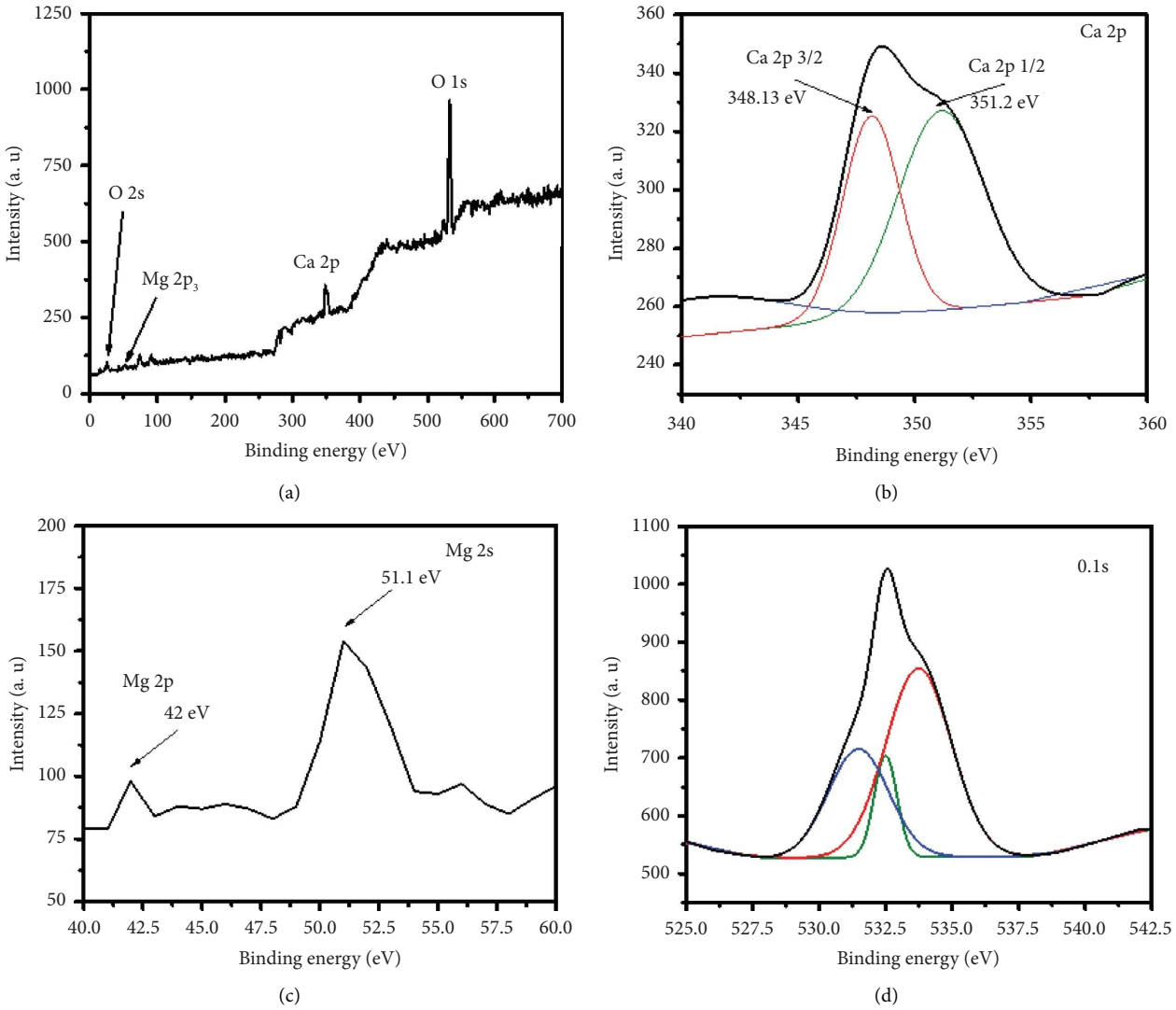

Figure 3: XPS spectra of (a) survey, (b) Ca-2p, (c) Mg-2p, and (d) O-1s for CaO.MgO nanosorbent.

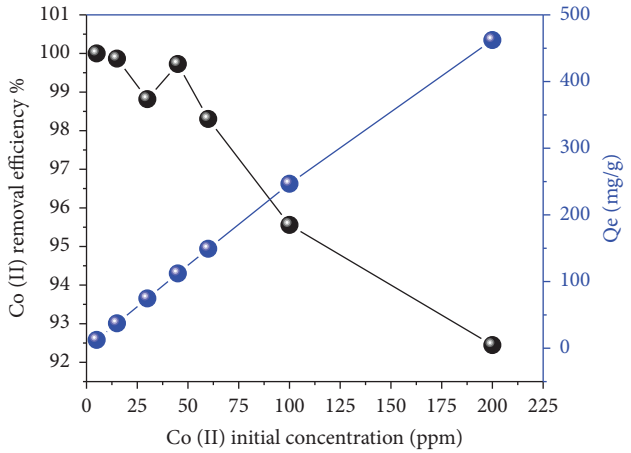

Figure 4: Evolution of the adsorption rate as a function of Co (II) initial concentration by CaO.MgO nanosorbent.

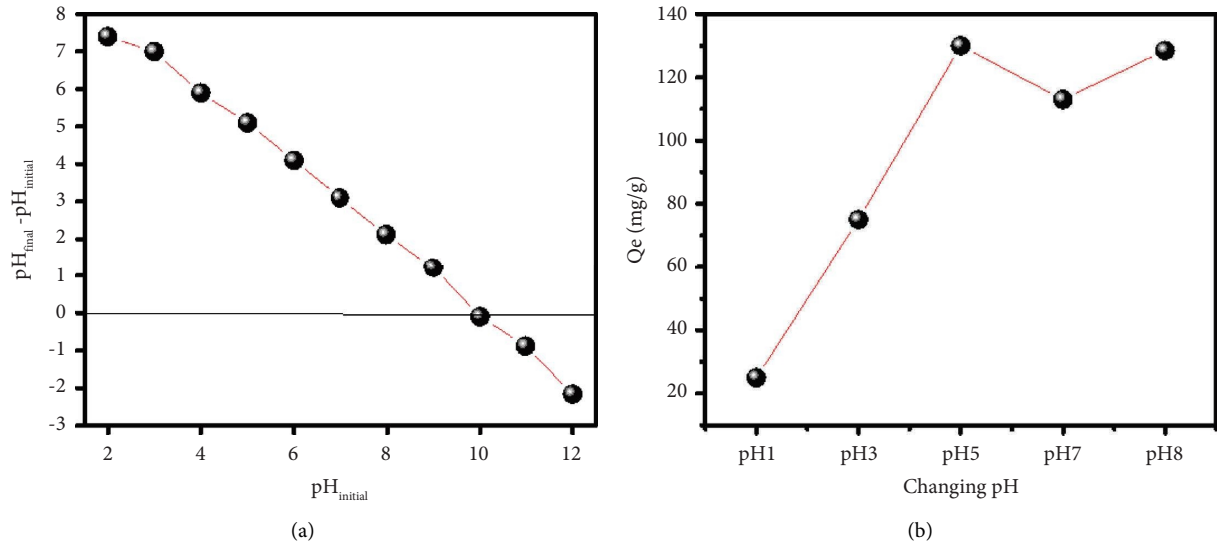

Figure 5: (a) pH point of zero charge (pHpzc) and (b) effect of pH on the removal capacity (mg/g) of Co (II) onto CaO.MgO nanosorbent.

the experimental adsorption kinetics data. It states that the rate of adsorption sites' occupation is related to the square of the number of available sites. The formula denoting the PSO linear model's form is given in Table 1. Figure 6(c) depicts the nonlinear curves of Q_t vs. t. The extremely high R^2 value of 0.9999 is obtained using the model parameters calculated in Table 1. The results reveal that the pseudo-second-order equation provides a perfect match compared to the pseudo-first-order model. It can be seen that the differences between the model estimated Q_{max} values and the experimental Q_{max} values for the studied Co (II) concentrations are negligible. Hence, the best fit of the pseudo-second-order model implies the concentration of Co (II) in the solution, and the accessible active sites onto CaO.MgO nanosorbent can be used to explain the intrinsic kinetic adsorption constant mathematically [58–60]. Figure 6(d) depicts the intraparticle diffusion plot. It can be observed that the adsorption process occurs upon two distinct stages. The first stage reflects the transport of Co(II) ions from the bulk solution through the boundary layer to the surface of CaO.MgO nanosorbent, whereas the second stage manifests the equilibrium state in which intraparticle diffusion starts to diminish due to low Co(II) concentration.

3.2.4. Adsorption Modeling of Co (II) onto CaO.MgO Nanosorbent. The maximum amount of Co (II) (Q_{max}) adsorbed by the sorbent presents another critical feature for evaluating the high adsorption ability displayed by CaO.MgO nanocomposite. To assess its absorption capability, the adsorption data have been evaluated using several adsorption isotherms models, namely Freundlich and Langmuir as illustrated in Figures 7(a) and 7(b). The formulas corresponding to each isotherm model and the computed parameters are given in Table 2.

As can be noted from the isotherm graphs and the experimental data for Co (II) adsorption over CaO.MgO nanosorbent, the Langmuir adsorption isotherm has the highest $R^2 = 0.9979$. The equilibrium value of R_L is around 0.0021, suggesting a desirable adsorption equilibrium [63]. These findings indicate that the Langmuir adsorption isotherm curve is more accurate to fit the experimental data. The greatest sorption capacity of CaO.MgO nanosorbent for Co (II) is found to be 469.5 mg.$\cdot g^{-1}$, as given in Table 2.

The capability of CaO.MgO to adsorb cobalt ions from aqueous media was compared to other adsorbents previously described in the literature. As shown in Table 3, the obtained Ca-MgO nanosorbent has a greater capacity for Co (II) ions removal than previously reported sorbents, indicating its potential as a promising nanosorbent for the removal of cobalt ions from aqueous media.

3.3. Adsorption Mechanism. FTIR analysis has been assessed to propose a plausible mechanism for Co (II) ions adsorption onto CaO.MgO nanosorbent. The FTIR spectra before and after Co (II) ions adsorption are shown in Figure 8(a). The position of the OH stretching vibration band has been shifted significantly, as illustrated in Figure 7(a), indicating that Co (II) interacts with the OH in MgO to establish an O–Co bond. The displacement of the CaO vibration band at 871 cm^{-1} confirms the interaction between Co (II) ions and the oxygen of CaO [39]. In addition, the FTIR bands of unidentate carbonate onto the particles' surface are shifted after Co (II) ions adsorption. This finding indicates that the unidentate surface carbonate

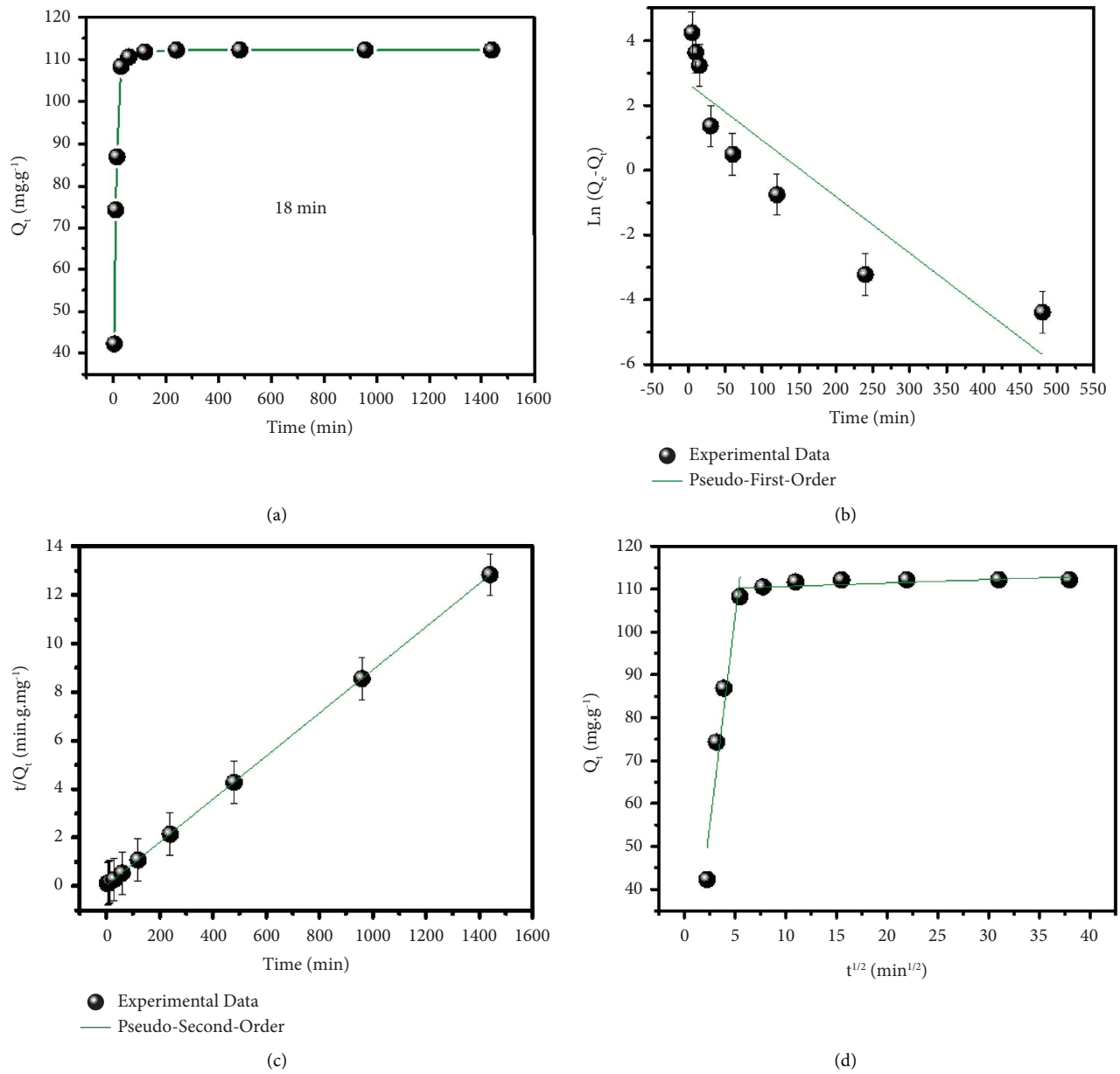

Figure 6: Effects of duration time (a), PFO (b), PSO adsorption kinetics models (c), and intraparticle diffusion of Co (II) onto CaO.MgO nanosorbent.

Table 1: Kinetics models for Co (II) adsorption onto CaO.MgO nanosorbent.

Kinetics model	Kinetic equation	Parameters	Values
PFO [59]	$\ln(Q_e - Q_t) = \ln q_e - k_1 t$	Q_e (mg/g)	14.38 ± 1.07
		K_1 (min^{-1})	0.0174 ± 0.19
		R^2	0.9038
PSO [59]	$t/Q_t = [1/k_2 Q_e^2] + (1/Q_e)t$	Q_m (exp) (mg/g)	113.5 ± 1.24
		Q_m (cal) (mg/g)	112.49
		K_2 (g/mg.·min)	0.0029 ± 0.41
		h_0 (mg/g·min)	36.95
		$t_{1/2}$ (min)	3.044
		R^2	0.9999
Intraparticle diffusion [60]	$q_t = k_{dif} t^{1/2} + C$	K_{dif1}(mg. $min^{1/2}$/g)	19.51
		C_1	5.997
		R^2	0.9671
		K_{dif2} (mg. $min^{1/2}$/g)	0.816
		C_2	109.8
		R^2	0.6783

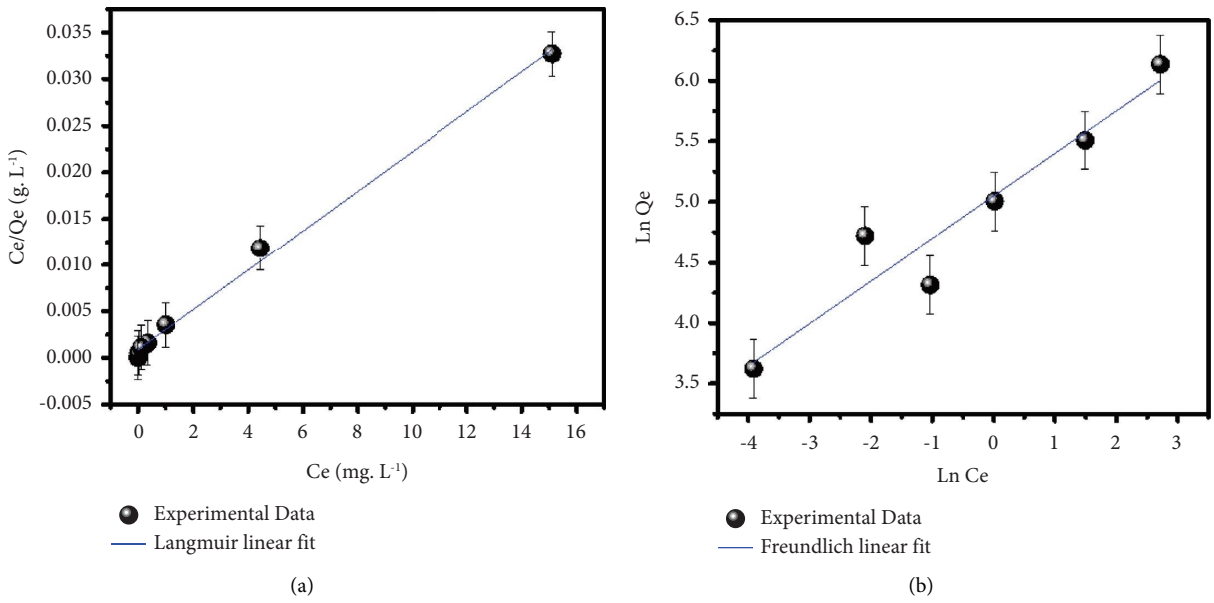

Figure 7: Experimental adsorption data fitted with the Langmuir (a) and Freundlich (b) models.

Table 2: Equilibrium isotherm models for Co (II) adsorption onto CaO.MgO nanosorbent.

Equilibrium model	Linear form	Parameters	Values
Langmuir [61]	$C_e/q_e = 1/q_m K_L + C_e/q_m$	q_m (mg/g)	469.5 ± 4.84
		K_L (mg/g)	$0.2341 \pm 1.22 \times 10^{-3}$
		R_L (L/mg)	0.0021
		R^2	0.9979
Freundlich [62]	$\ln q_e = \ln K_F + (1/n)\ln C_e$	N	2.847 ± 0.128
		K_F (L/mg)	155.9 ± 5.91
		R^2	0.9568

Table 3: Adsorption capability of various cited sorbents for the Co (II) ions removal.

Adsorbents	Adsorption capacity (mg/g)	Time (min.)	References
Ion-imprinted polymer	23.1	10	[64]
Nanosponge biopolymer	7.8	80	[18]
Carbon@UiO-66 bio-nanocomposite	44.5	20	[65]
Modified chitosan nanocomposites	43.9	60	[66]
GO-BSA membrane	180	80	[20]
Doped glycerol	117.9	70	[67]
Carbon-modified zirconia/spinel ferrite	82.5	60	[68]
Amination graphene oxide	116.3	5	[69]
Ca-MgO	469.5	18	Present study

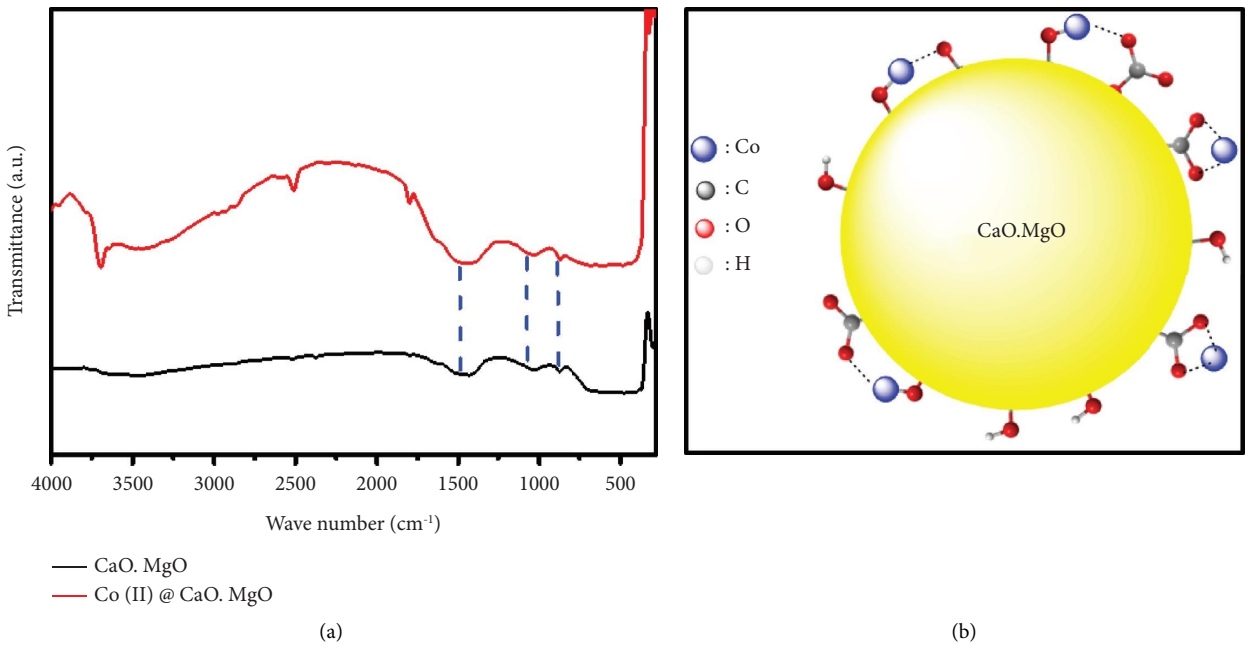

Figure 8: FTIR spectra of CaO.MgO nanosorbent before (a) and after Co (II) adsorption and (b) the proposed adsorption mechanism.

may have been involved in the removal of Co (II) ions. Wu et al. established by FTIR and XPS analyses that the surface monodentate carbonate species contributed to the As (V) adsorption mechanism [41]. Figure 8(b) illustrates the plausible adsorption mechanism of Co (II) ions onto the CaO.MgO nanosorbent.

4. Conclusion

CaO.MgO nanosorbent fabricated through a sol-gel method exhibits remarkable adsorption ability to remove Co (II) from an aqueous solution effectively. Structural, microstructural, and physicochemical characterizations indicate the formation of CaO.MgO composite with a relatively high surface area (50 m^2/g) and pore size (11.79 nm), and porous nanostructure formed the irregular spherical particles (20 nm), besides the presence of functional groups at the particles' surface. The adsorption kinetics process fits well with the pseudo-second-order kinetic model (PSO). The adsorption of Co (II) obeys the Langmuir adsorption isotherm, with an excellent removal capacity of 469.5 mg/g and a very high correlation coefficient ($R^2 = 0.9979$). This study demonstrates that the bio-fabricated cost-effective CaO.MgO nanosorbent possesses superior characteristics for the removal of Co (II) in an aqueous solution and can be assessed for the removal of other heavy metal ions and organic pollutants.

Data Availability

The data used it to support the findings of this research are available from of the main author upon request.

Conflicts of Interest

The authors declare that they have no conflicts of interest.

Authors' Contributions

The study plan, preparation of materials, data collection, and analyses were carried out by the authors with their contributions throughout the reviewing process. All authors read and approved the final work before it was published.

References

[1] D. G. Barceloux and D. Barceloux, *Journal of Toxicology - Clinical Toxicology*, vol. 37, no. 2, pp. 201–216, 1999.

[2] J. H. Bieleman, "Progress in the development of cobalt free drier systems," in *Macromolecular Symposia*Wiley Online Library, Hoboken, New Jersey, USA, 2002.

[3] S. Roberts and G. Gunn, *6. Cobalt Critical Metals Handbook*, p. 122, Wiley, Hoboken, NJ, USA, 1988.

[4] B. Ghiban, "Cobalt based alloys for dental applications," in *Key Engineering Materials*Trans Tech Publ, Switzerland, 2014.

[5] J. P. Mercier, G. Zambelli, and W. Kurz, *Introduction to Materials Science*, Elsevier, Amsterdam, Netherlands, 2012.

[6] D. Joksimovic, I. Tomic, A. R. Stankovic, M. Jovic, and S. Stankovic, "Trace metal concentrations in Mediterranean blue mussel and surface sediments and evaluation of the mussels quality and possible risks of high human consumption," *Food Chemistry*, vol. 127, no. 2, pp. 632–637, 2011.

[7] A. G. Ebadi, M Toughani, A Najafi, and M Babaee, "A brief overview on current environmental issues in Iran," *Central Asian Journal of Environmental Science and Technology Innovation*, vol. 1, no. 1, pp. 1–11, 2020.

[8] P. Sharma, S. Kumar, and A. Pandey, "Bioremediated techniques for remediation of metal pollutants using metagenomics approaches: a review," *Journal of Environmental Chemical Engineering*, vol. 9, no. 4, Article ID 105684, 2021.

[9] X. Zeng and J. Li, "On the sustainability of cobalt utilization in China," *Resources, Conservation and Recycling*, vol. 104, pp. 12–18, 2015.

[10] S. Rengaraj and S.-H. Moon, "Kinetics of adsorption of Co (II) removal from water and wastewater by ion exchange resins," *Water Research*, vol. 36, no. 7, pp. 1783–1793, 2002.

[11] N. B. Haq, K. Rubina, and A. H. Muhammad, "Biosorption of Pb (II) and Co (II) on Red Rose Waste Biomass," *iranian journal of chemistry & chemical engineering-international english edition*, vol. 30, no. 4, pp. 81–88, 2011.

[12] M. A. Islam, D. W. Morton, B. B. Johnson, B. K. Pramanik, B. Mainali, and M. J. Angove, "Opportunities and constraints of using the innovative adsorbents for the removal of cobalt (II) from wastewater: a review," *Environmental Nanotechnology, Monitoring & Management*, vol. 10, pp. 435–456, 2018.

[13] R. Mozrzymas, "Trace elements in human health," *Recent Adv Trace Elem*, vol. 26, pp. 373–402, 2018.

[14] T. Ma, S. Sun, G. Fu et al., "Pollution exacerbates China's water scarcity and its regional inequality," *Nature Communications*, vol. 11, no. 1, pp. 650–659, 2020.

[15] S. Seif, S. Marofi, and S. Mahdavi, "Effect of MgO and montmorillonite nanoparticles on removal behavior of cobalt," *Desalination and Water Treatment*, vol. 228, pp. 242–252, 2021.

[16] A. Rodríguez, P. Saez, E. Diez, J. M. Gomez, J. Garcia, and I. Bernabe, "Highly efficient low-cost zeolite for cobalt removal from aqueous solutions: characterization and performance," *Environmental Progress & Sustainable Energy*, vol. 38, no. s1, pp. S352–S365, 2019.

[17] E. A. Abdelrahman, Y. Abou El-Reash, H. M. Youssef, Y. H. Kotp, and R. Hegazey, "Utilization of rice husk and waste aluminum cans for the synthesis of some nanosized zeolite, zeolite/zeolite, and geopolymer/zeolite products for the efficient removal of Co (II), Cu (II), and Zn (II) ions from aqueous media," *Journal of Hazardous Materials*, vol. 401, Article ID 123813, 2021.

[18] A. L. Taka, E. Fosso-Kankeu, K. Pillay, and X. Y. Mbianda, "Removal of cobalt and lead ions from wastewater samples using an insoluble nanosponge biopolymer composite: adsorption isotherm, kinetic, thermodynamic, and regeneration studies," *Environmental Science and Pollution Research*, vol. 25, no. 22, pp. 21752–21767, 2018.

[19] M. H. Dehghani, K. Yetilmezsoy, M. Salari, Z. Heidarinejad, M. Yousefi, and M. Sillanpaa, "Adsorptive removal of cobalt (II) from aqueous solutions using multi-walled carbon nanotubes and γ-alumina as novel adsorbents: modelling and optimization based on response surface methodology and artificial neural network," *Journal of Molecular Liquids*, vol. 299, Article ID 112154, 2020.

[20] S. Joshi, H. Singh, S. Sharma, P. Barman, A. Saini, and G. Verma, "Synthesis and characterization of graphene oxide-bovine serum albumin conjugate membrane for adsorptive removal of Cobalt (II) from water," *International journal of Environmental Science and Technology*, vol. 18, no. 12, pp. 3915–3928, 2021.

[21] W. S. Chai, J. Y. Cheun, P. S. Kumar et al., "A review on conventional and novel materials towards heavy metal adsorption in wastewater treatment application," *Journal of Cleaner Production*, vol. 296, Article ID 126589, 2021.

[22] Z. Iqbal, M. S. Tanweer, and M. Alam, "Recent advances in adsorptive removal of wastewater pollutants by chemically modified metal oxides: a review," *Journal of Water Process Engineering*, vol. 46, Article ID 102641, 2022.

[23] Y. Wang, Y. Tong, X. Xu, and L. Zhang, "Developed magnetic multiporous 3D N-Co@ C/HCF as efficient sorbent for the extraction of five trace phthalate esters," *Analytica Chimica Acta*, vol. 1054, pp. 176–183, 2019.

[24] A. Kumar, H. Joshi, and A. Kumar, "Remediation of arsenic by metal/metal oxide based nanocomposites/nanohybrids: contamination scenario in groundwater, practical challenges, and future perspectives," *Separation and Purification Reviews*, vol. 50, no. 3, pp. 283–314, 2021.

[25] N. Nik Abdul Ghani, M. Jami, and M. Alam, "The role of nanoadsorbents and nanocomposite adsorbents in the removal of heavy metals from wastewater: a review and prospect," *Pollution*, vol. 7, no. 1, pp. 153–179, 2021.

[26] S. Mahdavi, Z. Tarhani, A. H. Sayyahzadeh, and E. Naderi Peikam, "Effect of nano-MgO, biochar and humic acid on boron stabilization in soil in bath and leaching columns," *Soil and Sediment Contamination: International Journal*, vol. 29, no. 6, pp. 595–612, 2020.

[27] M. Fernandes, K. Rb Singh, T. Sarkar, P. Singh, and R. Pratap Singh, "Recent applications of magnesium oxide (MgO) nanoparticles in various domains," *Advanced Material Letters*, vol. 11, no. 8, pp. 1–10, 2020.

[28] A. Modwi, L. Khezami, K. K. Taha, and H. Idriss, "Flower buds like MgO nanoparticles: from characterisation to indigo carmine elimination," *Zeitschrift für Naturforschung A*, vol. 73, no. 11, pp. 975–983, 2018.

[29] L. Khezami, K. K. Taha, and A. Modwi, "Efficient removal of cobalt from aqueous solution by zinc oxide nanoparticles: kinetic and thermodynamic studies," *Zeitschrift für Naturforschung A*, vol. 72, no. 5, pp. 409–418, 2017.

[30] H. Idriss, "Decolorization of malachite green in aqueous solution via MgO nanopowder," *Journal of Optoelectronic and Biomedical Materials*, vol. 13, no. 4, pp. 183–192, 2021.

[31] H. Idriss, A. Alakhras, and H. El Khair, "Malachite green removal from aqueous solutions by MgO (86%). Se (7%). Te (7%) nanocomposites," *Chalcogenide Letters*, vol. 18, no. 10, pp. 629–638, 2021.

[32] A. Modwi, M. Abbo, E. Hassan, O. Al-Duaij, and A. Houas, "Adsorption kinetics and photocatalytic degradation of malachite green (MG) via Cu/ZnO nanocomposites," *Journal of Environmental Chemical Engineering*, vol. 5, no. 6, pp. 5954–5960, 2017.

[33] G. N. Kopanati, S. Seethamraju, P. C. Ramamurthy, and G. Madras, "A Surlyn/magnesium oxide nanocomposite as an effective water vapor barrier for organic device encapsulation," *RSC Advances*, vol. 5, no. 41, pp. 32580–32587, 2015.

[34] M. Bashir and S. Haripriya, "Assessment of physical and structural characteristics of almond gum," *International Journal of Biological Macromolecules*, vol. 93, pp. 476–482, 2016.

[35] A. Roy, S. S. Gauri, M. Bhattacharya, and J. Bhattacharya, "Antimicrobial activity of CaO nanoparticles," *Journal of Biomedical Nanotechnology*, vol. 9, no. 9, pp. 1570–1578, 2013.

[36] A. Modwi, M. A. Abbo, E. A. Hassan, and A. Houas, "Effect of annealing on physicochemical and photocatalytic activity of Cu5% loading on ZnO synthesized by sol–gel method," *Journal of Materials Science: Materials in Electronics*, vol. 27, no. 12, pp. 12974–12984, 2016.

[37] J. B. Condon, *Surface Area and Porosity Determinations by Physisorption: Measurements and Theory*, Elsevier, Amsterdam, Netherlands, 2006.

[38] V. J. Inglezakis, S. G. Poulopoulos, and H. Kazemian, "Insights into the S-shaped sorption isotherms and their dimensionless forms," *Microporous and Mesoporous Materials*, vol. 272, pp. 166–176, 2018.

[39] S. Xu, Z. Zhong, W. Liu, H. Deng, and Z. Lin, "Removal of Sb (III) from wastewater by magnesium oxide and the related

mechanisms," *Environmental Research*, vol. 186, Article ID 109489, 2020.

[40] Y. Liu, Q. Li, S. Gao, and J. K. Shang, "Exceptional as (III) sorption capacity by highly porous magnesium oxide nanoflakes made from hydrothermal synthesis," *Journal of the American Ceramic Society*, vol. 94, no. 1, pp. 217–223, 2011.

[41] P.-Y. Wu, Y. P. Jiang, Q. Y. Zhang, Y. Jia, D. Y. Peng, and W. Xu, "Comparative study on arsenate removal mechanism of MgO and MgO/TiO 2 composites: FTIR and XPS analysis," *New Journal of Chemistry*, vol. 40, no. 3, pp. 2878–2885, 2016.

[42] S. Taghavi Fardood, A. Ramazani, and S. Woo Joo, "Eco-friendly synthesis of magnesium oxide nanoparticles using Arabic Gum," *Journal of Applied Chemical Research*, vol. 12, no. 1, pp. 8–15, 2018.

[43] Y. Y. Margaretha, H. S. Prastyo, A. Ayucitra, and S. Ismadji, "Calcium oxide from Pomacea sp. shell as a catalyst for biodiesel production," *International Journal of Energy and Environmental Engineering*, vol. 3, no. 1, pp. 33–39, 2012.

[44] H.-H. Huang, W.-C. Shih, and C.-H. Lai, "Nonpolar resistive switching in the Pt/MgO/Pt nonvolatile memory device," *Applied Physics Letters*, vol. 96, no. 19, Article ID 193505, 2010.

[45] J. Liu, "Conversion of Au (III)-polluted Waste Eggshell into Functional CaO/Au Nanocatalyst for Biodiesel Production," *Green Energy & Environment*, vol. 7, no. 2, 2020.

[46] I. Karuppusamy, M. S. Samuel, E. Selvarajan et al., "Ultrasound-assisted synthesis of mixed calcium magnesium oxide (CaMgO2) nanoflakes for photocatalytic degradation of methylene blue," *Journal of Colloid and Interface Science*, vol. 584, pp. 770–778, 2021.

[47] J. Rojas, M. Toro-Gonzalez, M. Molina-Higgins, and C. Castano, "Facile radiolytic synthesis of ruthenium nanoparticles on graphene oxide and carbon nanotubes," *Materials Science and Engineering: B*, vol. 205, pp. 28–35, 2016.

[48] M. Kapilashrami, J. Xu, K. V. Rao, L. Belova, E. Carlegrim, and M. Fahlman, "Experimental evidence for ferromagnetism at room temperature in MgO thin films," *Journal of Physics: Condensed Matter*, vol. 22, no. 34, Article ID 345004, 2010.

[49] L. Ge, Z. Peng, W. Wang et al., "gC 3 N 4/MgO nanosheets: light-independent, metal-poisoning-free catalysts for the activation of hydrogen peroxide to degrade organics," *Journal of Materials Chemistry*, vol. 6, no. 34, pp. 16421–16429, 2018.

[50] R. K. Schulze, M. A. Hill, R. D. Field, P. A. Papin, R. J. Hanrahan, and D. D. Byler, "Characterization of carbonated serpentine using XPS and TEM," *Energy Conversion and Management*, vol. 45, no. 20, pp. 3169–3179, 2004.

[51] B. Mustafa, A. Modwi, M. Ismail et al., "Adsorption performance and kinetics study of Pb (II) by RuO2–ZnO nanocomposite: construction and recyclability," *International journal of Environmental Science and Technology*, vol. 19, no. 1, pp. 327–340, 2022.

[52] S. O. Akpotu, P. N. Diagboya, I. A. Lawal et al., "Designer composite of montmorillonite-reduced graphene oxide-PEG polymer for water treatment: enrofloxacin sequestration and cost analysis," *Chemical Engineering Journal*, vol. 453, Article ID 139771, 2023.

[53] N. Esfandiar, R. Suri, and E. R. McKenzie, "Competitive sorption of Cd, Cr, Cu, Ni, Pb and Zn from stormwater runoff by five low-cost sorbents; Effects of co-contaminants, humic acid, salinity and pH," *Journal of Hazardous Materials*, vol. 423, Article ID 126938, 2022.

[54] K. Suwannahong, "Selective Chelating Resin for Copper Removal and Recovery in Aqueous Acidic Solution Generated from Synthetic Copper-Citrate Complexes from Bioleaching of E-Waste," *Adsorption Science & Technology*, vol. 2022, p. 158, Article ID 5009124, 2022.

[55] K. Low, C. Lee, and A. Leo, "Removal of metals from electroplating wastes using banana pith," *Bioresource Technology*, vol. 51, no. 2-3, pp. 227–231, 1995.

[56] D. Luo and J. Wei, "Upgrading sodium montmorillonite into a reactive internal curing agent for sustainable cement composites through non-ionic functionalization," *Composites Part B: Engineering*, vol. 242, Article ID 110076, 2022.

[57] B. Oladipo, E. Govender-Opitz, and T. V. Ojumu, "Kinetics, thermodynamics, and mechanism of Cu (II) ion sorption by biogenic iron precipitate: using the lens of wastewater treatment to diagnose a typical biohydrometallurgical problem," *ACS Omega*, vol. 6, no. 42, pp. 27984–27993, 2021.

[58] L. Khezami, N. Elamin, A. Modwi, K. K. Taha, M. Amer, and M. Bououdina, "Mesoporous Sn@ TiO2 nanostructures as excellent adsorbent for Ba ions in aqueous solution," *Ceramics International*, vol. 48, no. 4, pp. 5805–5813, 2022.

[59] S. K. Lagergren, "About the theory of so-called adsorption of soluble substances," *Sven. Vetenskapsakad. Handingarl*, vol. 24, pp. 1–39, 1898.

[60] S. H. Chien and W. R. Clayton, "Application of Elovich equation to the kinetics of phosphate release and sorption in soils," *Soil Science Society of America Journal*, vol. 44, no. 2, pp. 265–268, 1980.

[61] M. A. Al-Ghouti and M. M. Razavi, "Water reuse: brackish water desalination using Prosopis juliflora," *Environmental Technology & Innovation*, vol. 17, Article ID 100614, 2020.

[62] N. Ayawei, A. N. Ebelegi, and D. Wankasi, "Modelling and interpretation of adsorption isotherms," *Journal of Chemistry*, vol. 2017, pp. 1–11, Article ID 3039817, 2017.

[63] I. Langmuir, "The adsorption of gases on plane surfaces of glass, mica and platinum," *Journal of the American Chemical Society*, vol. 40, no. 9, pp. 1361–1403, 1918.

[64] R. Kang, L. Qiu, L. Fang et al., "A novel magnetic and hydrophilic ion-imprinted polymer as a selective sorbent for the removal of cobalt ions from industrial wastewater," *Journal of Environmental Chemical Engineering*, vol. 4, no. 2, pp. 2268–2277, 2016.

[65] H. Motaghi, "Simultaneous Adsorption of Cobalt Ions, Azo Dye, and Imidacloprid Pesticide on the Magnetic Chitosan/activated Carbon@ UiO-66 Bio-Nanocomposite: Optimization, Mechanisms, Regeneration, and Application," *Separation and Purification Technology*, vol. 248, Article ID 120258, 2021.

[66] S. M. Abdelbasir, A. M. El-Shewaikh, S. M. El-Sheikh, and O. I. Ali, "Novel modified chitosan nanocomposites for Co (II) ions removal from industrial wastewater," *Journal of Water Process Engineering*, vol. 41, Article ID 102008, 2021.

[67] A. Abdelfatah, O. F. Abdel-Gawad, A. M. Elzanaty, A. M. Rabie, and F. Mohamed, "Fabrication and optimization of poly (ortho-aminophenol) doped glycerol for efficient removal of cobalt ion from wastewater," *Journal of Molecular Liquids*, vol. 345, Article ID 117034, 2022.

[68] M. Abdel Maksoud, N. Sami, H. Hassan, M. Bekhit, and A. Ashour, "Novel adsorbent based on carbon-modified zirconia/spinel ferrite nanostructures: evaluation for the removal of cobalt and europium radionuclides from aqueous solutions," *Journal of Colloid and Interface Science*, vol. 607, pp. 111–124, 2022.

[69] F. Fang, L. Kong, J. Huang et al., "Removal of cobalt ions from aqueous solution by an amination graphene oxide nanocomposite," *Journal of Hazardous Materials*, vol. 270, pp. 1–10, 2014.